Delft University of Technology

An Analytical and Numerical Approach for Shear Failure of Pier-Wall Connections in Typical Dutch URM Buildings

Fusco, Daniela; Addessi, D.; Messali, F.; Rots, J. G.; Pampanin, S.

Important note
To cite this publication, please use the final published version (if applicable).
Please check the document version above.

An Analytical and Numerical Approach for Shear Failure of Pier-Wall Connections in Typical Dutch URM Buildings

Daniela Fusco, D. Addessi, F. Messali, J. G. Rots & S. Pampanin

Published online: 19 Sep 2022.

Submit your article to this journal

Article views: 38

View related articles

View Crossmark data

Taylor & Francis
Taylor & Francis Group

Check for updates

An Analytical and Numerical Approach for Shear Failure of Pier-Wall Connections in Typical Dutch URM Buildings

Daniela Fusco[a], D. Addessi [ID][a], F. Messali [ID][b], J. G. Rots[b], and S. Pampanin[a]

[a]Dipartimento di Ingegneria Strutturale e Geotecnica, Sapienza Università di Roma, Rome, Italy; [b]Department 3MD, Delft University of Technology, Delft, The Netherlands

ABSTRACT

Since the 1980s, calcium silicate element masonry has been commonly used in Dutch buildings, and vertical continuous joints have been usually located at the corner of perpendicular walls. Since the shear failure of these joints may significantly reduce the seismic performance of the flanged wall and therefore of the entire building, the assumption of rigid connection may be inaccurate, unlike for the traditional interlocking of bricks in running bond textures. In this paper, analytical and numerical approaches to study the failure of vertical joints in the seismic assessment of URM buildings are presented. The first part of the work focuses on two different numerical models to study the nonlinear behaviour of the vertical connection; the related critical numerical issues are then discussed. The second part introduces an analytical method able to estimate the lateral force–displacement curve of a flanged wall, which considers the possible failure of the connection. In particular, the method is derived from the section analysis approach developed for controlled rocking deformable systems. The comparison between the numerical simulations and the analytical method proves the capacity of the latter to provide a quick but sufficiently accurate estimate of the force–displacement curve of a URM U-Shaped wall.

1. Introduction

The premature failure of connections between perpendicular walls was observed in a number of strong earthquakes (Parisi and Augenti 2013a), which showed that the joints play an important role in the seismic response of Unreinforced Masonry (URM) structures. Especially, this work focuses on the failure of vertical continuous connections in typical Dutch URM buildings. Dutch Unreinforced Masonry (URM) terraced houses are typically composed of facades with large openings and slender piers, connected at corners with transverse walls. A large number of URM terraced houses have window banks made of timber elements structurally not connected to the masonry, and the contribution of spandrels to the seismic response is considered negligible. An example of a real building lacking structural spandrels is shown in Figure 1.

The strength of the connections between the transverse main wall and piers influences the seismic capacity of the flanged walls, and therefore of the whole building. Before 1980, calcium silicate (CS) bricks with interlocking of the units at the corners were commonly used in building practice. Since the 1980s, large CS elements, having in-plane dimensions of 400×300 mm^2 or larger, gradually replaced the traditional small CS bricks (about

210×70 mm^2) to accelerate the construction process. At the corners between walls and piers, the connection is provided by a continuous vertical joint, with horizontal steel ties at the bed-joint level. A schematic figure of the flanged "U-Shaped" wall is shown in Figure 2. The continuous vertical connections are weaker than the traditional toothed ones and their sliding shear failure may considerably decrease the seismic capacity of the structure. For this reason, the assumption of rigid connection, usually holding in case of interlocking of the bricks, may be inappropriate in case of vertical connection (Fusco et al. 2021, 2022; Rots et al. 1997).

Raijmakers and Van der Pluijm (1992) conducted an experimental campaign to test the lateral capacity of a U-Shaped element composed of piers and walls linked through a continuous connection. In the following years, the seismicity in the Netherlands induced by the gas extraction raised interest in the study of seismic vulnerability of typical Dutch URM buildings and several experimental campaigns from the material level up to the structural scale have been carried out. In particular, a full-scale two-storey building was tested at Delft University of Technology to evaluate the seismic capacity of these structures (Esposito et al. 2019, 2017; Mariani et al. 2017; Messali et al. 2018). In recent

Figure 1. Typical Dutch Unreinforced Masonry (URM) terraced houses [http://www.bestaandewijk.nl/tag/jaren-60-wijk/ - Roel Simons (photographer)].
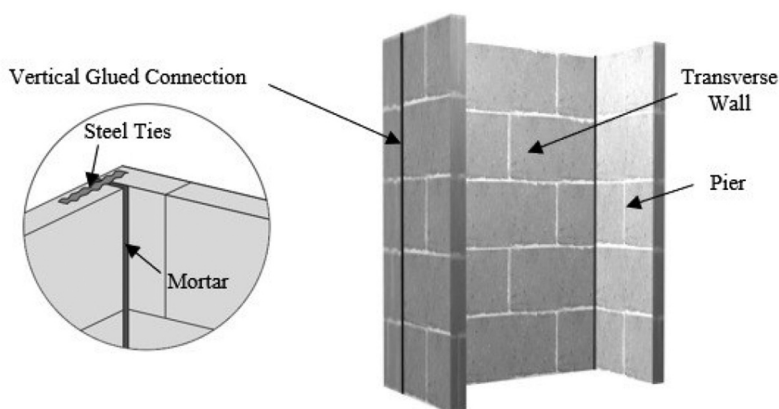

Figure 2. Pier-main wall system with calcium silicate elements and continuous vertical connections (Fusco et al. 2022).

years, the out-of-plane seismic performance of U-shaped elements was studied at the laboratory of Eucentre (Kallioras, Grottoli, and Graziotti 2020).

Moreover, several procedures were developed to evaluate the seismic capacity of URM buildings (Calderini, Cattari, and Lagomarsino 2008; Magenes and Penna 2011; Sacco, Addessi, and Sab 2018). Among them, the finite element method (FEM) is the most commonly adopted to perform nonlinear analyses. Different scales of the analysis can be distinguished for masonry modelling, that is micromechanical, macromechanical, macroelement based and multiscale models (Addessi et al. 2014; Calderini and Lagomarsino 2008; Lourenco 1996, 2002; Parisi, Balestrieri, and Asprone 2016). If on the one hand the numerical modelling of the URM structures allows to analyse the behaviour of complex structures under seismic loads, on the other hand a detailed description of the masonry microstructure would require high computational efforts, which may be unsustainable in engineering practice. Therefore, the development of simplified analytical methods can give an

effective tool for the preliminary analysis and control of the numerical results. Several analytical methods were also developed to estimate the force capacity of in-plane-loaded unreinforced masonry single walls (Benedetti and Steli 2008; Parisi and Augenti 2013b; Petry and Beyer 2015), but those were not implemented for flanged walls with continuous vertical joints.

This work aims to propose an analytical and numerical method to analyze the influence of the connection failure on the seismic capacity of typical Dutch URM buildings built after the 1980s. Section 2 proposes two alternative numerical approaches selected to describe the nonlinear behaviour of the continuous vertical connection, highlighting the issues related to the numerical modelling of joint shear failure (Fusco et al. 2021, 2022). In Section 3, an analytical method is proposed to derive the force–displacement curve of a flanged wall with a continuous vertical joint. This method is based on the procedure originally developed for the PREcast Seismic Structural System (PRESSS) post-tensioned rocking-dissipative technology, and elaborated by

a research team of the University of California, San Diego, to analytically calculate the force–displacement curve of the rocking mechanism of a deformable body (NZCS 2010; Pampanin 2005; Pampanin, Priestley, and Sritharan 2001; Priestley et al. 1999) as opposed to the traditional rigid body rocking theory (Housner 1963). In the years, the procedure, referred to as Monolithic Beam Analogy (MBA), has been adopted and successfully validated for a wide range of precast concrete, steel, laminated timber and masonry rocking systems (Christopoulos et al. 2002; Newcombe et al. 2008; Palermo 2004; Palermo et al. 2005; Palermo, Pampanin, and Carr 2005; Palermo, Pampanin, and Marriott 2007; Sansoni 2021). In this work, the method is extended and applied to a flanged URM wall, allowing to capture both the single wall rocking and the coupled (thus post-sliding) rocking mechanism. Section 4 summarizes the conclusions of the paper.

2. Finite element modelling of continuous vertical connections

The interlocking of masonry bricks provides a strong connection between walls at the corner of masonry structures, which is usually modelled as rigid in numerical models. In case of typical Dutch URM buildings built after 1980, this assumption may lead to overestimate the seismic capacity of the structures due to the possible shear failure of the vertical connection between the main wall and piers. Experimental research performed by Raijmakers and Van der Pluijm (1992) investigated the seismic performance of a masonry sub-assembly with continuous vertical connections: a U-shaped structure, composed of the main wall and two perpendicular piers, was tested under lateral loading to study the occurrence of possible failure mechanisms. This section focuses on the three tests with calcium silicate elements and continuous vertical joints at the corners without the horizontal steel ties at the bed-joint level. The experimental test consisted in the application of an initial vertical load on top of the main wall, followed by a monotonically increasing horizontal load. The dead weight of the floor is applied only to the transverse wall,

because this load condition simulates reinforced concrete floors spanning in between the transverse walls, which is representative of the floor system in typical Dutch terraced houses. The stabilizing moment of the structure was given by the self-weight of the components and the vertical load applied at the top of the wall. Figure 3 summarizes the three potential failure mechanisms of the U-shaped structure investigated by the experimental test: (a) the rocking mechanism of the structure, followed by compression failure at toes of the pier; (b) the diagonal cracking/compression failure of the pier; and (c) the shear failure of the joint. When dealing with strong connections, as in case of the interlocking of bricks, either the mechanisms (a) or (b) prevail. In particular, the compressive failure is associated with sub-vertical cracks at the wall toes. It typically occurs for large rotations of the piers determined by the rocking motion, but it may also precede the activation of the rocking mechanism in case of high vertical stresses. When the connections are weak, as in case of continuous connections, the brittle failure of the joint (c) determines a sudden reduction of the capacity of the structure for lower horizontal forces than those related to the pier failure (Rots et al. 1997). In case of continuous vertical connections in typical Dutch buildings, tensile failure is prevented by the presence of steel anchors embedded in the bed-joint. Due to their flat geometry, such anchors have a low shear stiffness and strength and for this reason such contribution to the overall shear strength of the connection is neglected. On the other hand, their tensile strength is usually able to prevent the tensile opening of the joint. For this reason, the tensile failure of the joint and the consequent detachment of the pier is neglected.

The results of the experimental test are shown in Figures 7 and 8 (Rots et al. 1997).

2.1. Constitutive laws for continuous vertical connection

The continuous vertical connections between piers and walls are modelled through interface elements with non-linear behaviour to simulate the potential shear failure mechanism of the joint. The interface elements are
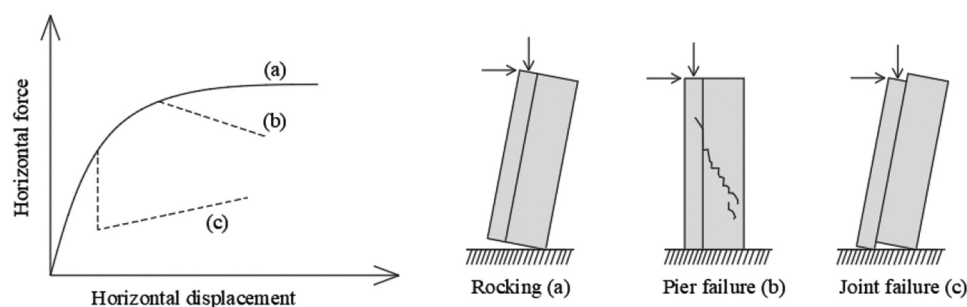

Figure 3. Failure mechanisms of a U-Shaped wall (Fusco et al. 2022; Rots et al. 1997).

characterized by cracking in tension along the normal direction "n" of the interface (perpendicular to the joint plane) and sliding in shear along the tangential direction "t". The tensile constitutive law is defined in terms of normal traction versus normal relative displacement, where the peak and softening phase are characterized by the tensile strength f_t and Mode I fracture energy G_f^I. In this work, a linear elastic constitutive law was adopted for the tensile/cracking behaviour of the joint. In addition, two alternative laws were selected among the proposed constitutive models to simulate the shear failure of the joint and compared among each other: a Coulomb friction model and a nonlinear elastic formulation. The Coulomb failure criterion is defined by the cohesion c_u and friction angle ϕ through the following formula (Fusco et al. 2022):

$$|t_t| \leq c_u - t_n \, tan\phi \qquad (1)$$

where the traction along the interface in normal and tangential direction are expressed by t_n and t_t, respectively. As known, in this formulation, the shear yield limit function depends on the stress in the normal direction. The nonlinear behaviour is governed by the cohesion softening curve and Mode II fracture energy G_f^{II}, as illustrated in Figure 4. The failure criterion reduces to dry friction when the cohesion softening is completed. The dilatancy angle may be defined equal to the friction angle in case of associated plasticity, whereas, if the dilatancy is assumed lower than the friction, a non-associated plasticity is formulated (DIANA FEA 2019).

As mentioned above, the Coulomb failure criterion is characterized by a coupled response in the shear and normal direction of the interface. This may complicate the convergence of the analyses when the brittle failure of the interface occurs, especially in case of non-associated plasticity where the stiffness matrix is non-symmetric. The adoption of an alternative nonlinear elastic model, although less consistent with the actual nonlinear mechanisms exhibited by the joint, was then explored. This constitutive law separately defines the behaviour in the two orthogonal directions, defining two uncoupled relative displacement-traction diagrams for the normal and tangential direction, respectively. The resulting diagonal stiffness matrix improves the robustness of the model, speeding up the convergence of the analysis (Fusco et al. 2022).

2.2. Numerical application

The U-Shaped structure tested by Raijmakers and Van der Pluijm (1992) was modelled adopting both plane stress (2D-model) and solid finite elements (3D-model), as illustrated in Figure 5. 4-node quadrilateral isoparametric elements with a 2 × 2 Gauss integration scheme, and interface elements with linear interpolation of the displacements, were used in the 2D-model. Conversely, 8-node isoparametric solid brick elements with 2x2x2 Gauss integration and linear interpolation interface elements were selected for the 3D-Model. In both 2D and 3D models, the mesh size was set equal to 100 mm following a sensitivity analysis of the numerical model. The Calcium Silicate masonry was modelled with linear elastic finite elements, as suggested in literature (Rots et al. 1997), with Young's modulus equal to 5000 N/mm² and a Poisson's ratio to 0.12. To simulate the rocking mechanism, boundary interface (contact surfaces) elements with no-tension response were introduced at the base section in between the masonry elements and the fixed supports. A constant vertical load was applied at the top of the wall to simulate the presence of the floor. A displacement-controlled analysis was performed by applying a monotonically increasing displacement on top of the wall as shown in Figure 5. For the 3D-Model, all the nodes located at the upper edge of the wall were connected by tying elements, which connect rigidly the translational degree of freedom in the horizontal x-axis of all nodes. The prescribed displacement in the x-direction is applied to the master joint of the tying elements so that all the slave nodes undergo the same horizontal displacement. According to this constraint and load conditions, both the connections between the transversal wall and the flanges are compressed in the
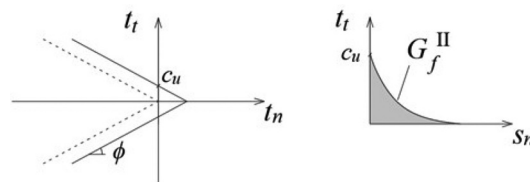

Figure 4. Coulomb friction model for shear stresses (Fusco et al. 2022; Rots et al. 1997).
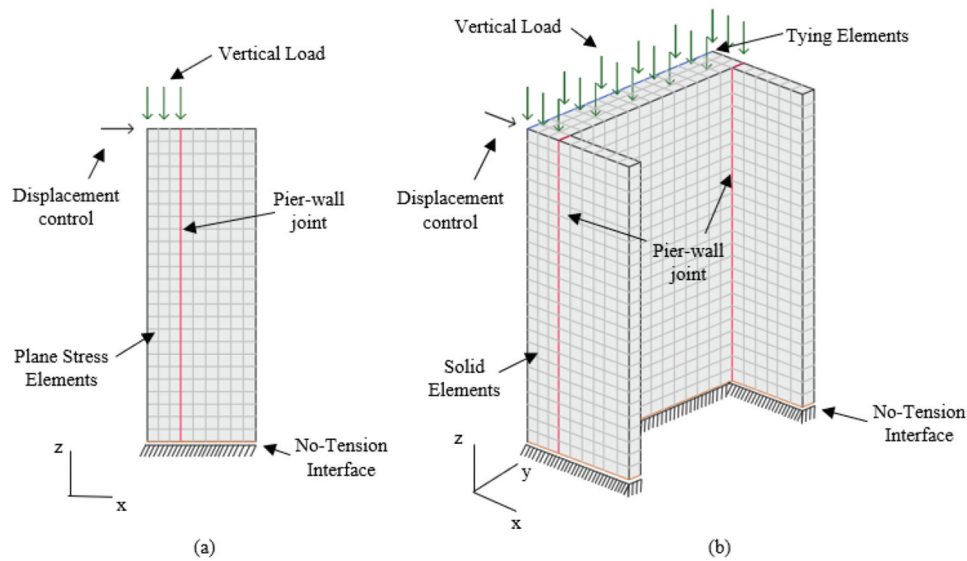
Figure 5. Model of the pier-main wall: 2D-model (a) and 3D-model (b) (Fusco et al. 2022).

same way. According to this constraint and load conditions, both the connections between the transversal wall and the flanges are compressed in the same way.

As mentioned in the previous section, the vertical connection was modelled through interface elements in between the wall and the pier, considering either the Coulomb friction model, or the nonlinear elastic model. The material parameters used for the Coulomb

Table 1. Vertical interface Coulomb friction model properties (Fusco et al. 2022; Rots et al. 1997).

Vertical Joint				
(Coulomb Friction)	Normal modulus	k_n	3125	N/mm²
	Shear modulus	k_t	1395	N/mm²
	Mode II fracture energy	G_f^{II}	0.05	N/m
	Cohesion	c_u	0.4	N/mm²
	Angle of friction	$tan\varphi$	0.75	-

friction law are summarized in Table 1, in accordance with the literature (Rots et al. 1997).

Regarding the nonlinear elastic constitutive law, an elastic behaviour was assumed in the normal direction, assuming no opening of the interface. In shear direction, a traction-relative displacement diagram was defined, as shown in Figure 6. The Coulomb friction failure criterion is capable of properly representing the physical behaviour of the interface, by coupling the shear strength to the normal stress. Since the latter varies along the height of the connection, also the shear strength assumes different values along the joint. On the opposite, the nonlinear elastic constitutive law defines a constant shear strength along the interface and this assumption requires to calibrate the maximum peak value.

Figure 6. Nonlinear elastic constitutive law: shear stress — relative displacement diagram (Fusco et al. 2022).

For this reason, three different maximum shear stresses were adopted, $t_{t,max}$ = 0.4 N/mm², 0.5 N/mm², 0.6 N/mm². A brittle behavior after the peak was defined to simulate the sudden propagation of the fracture along the joint. A calibrated value of the residual shear strength equal to 0.05 N/mm² was considered to simulate the residual friction along the interface after the complete degradation of the cohesion.

The results of the pushover analyses of the U-shaped structure obtained by the 2D-model are shown in Figure 7 (Fusco et al. 2022). Figure 7(a) illustrates the capacity curve obtained with the adoption of the Coulomb friction model, and Figure 7(b) that derived with the nonlinear elastic constitutive law. Both results are compared with the outcomes of the experimental test and with those of earlier simulations provided in Rots (Rots et al. 1997), where the arc-length method was

Figure 7. 2D-model capacity curves: Coulomb friction model (a) vs nonlinear elastic model (b) (Fusco et al. 2022).

Figure 8. 3D-model capacity curves: Coulomb friction model (a) vs nonlinear elastic model (b) (Fusco et al. 2022).

adopted to accurately describe the snap-back of the capacity curve, which corresponds to the propagation of the crack along the interface. The numerical methods described above cannot reproduce the snap-back due to the adopted displacement-controlled procedure.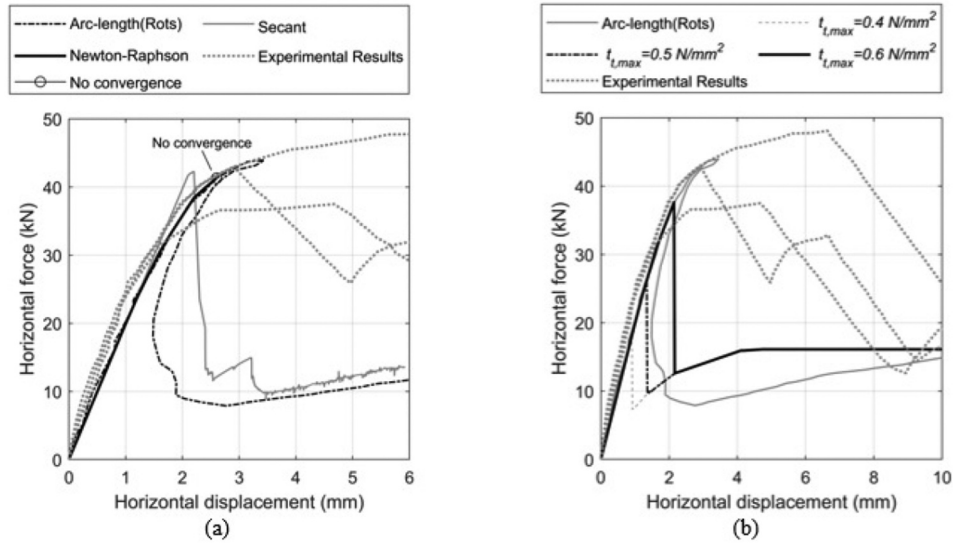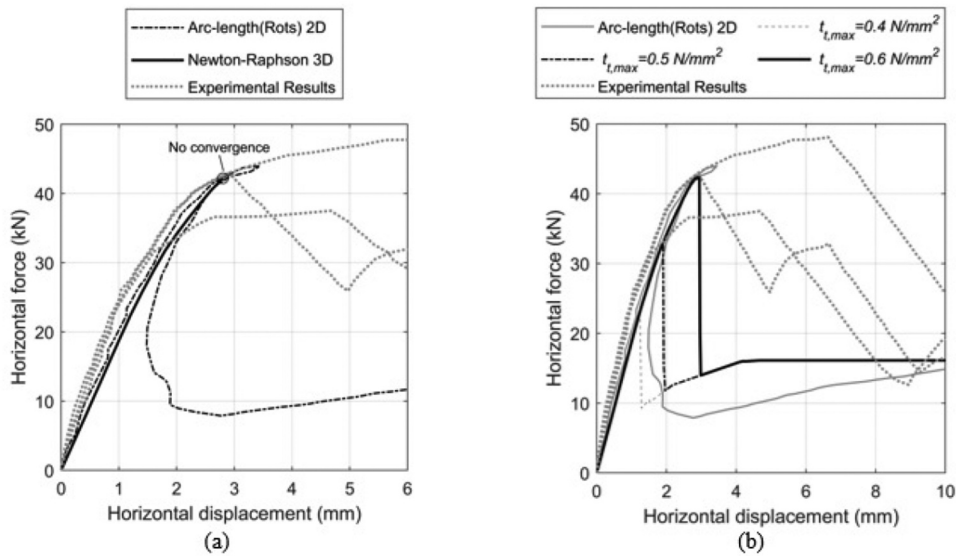 In case of Coulomb friction interface model, the numerical analyses showed great difficulty in reaching the convergence at the onset of the cracking, requiring a very high computational effort to overcome the peak of the capacity curve. Especially, the sudden propagation of the crack after the shear failure of the connection determined the divergence of the numerical solution, when the Newton-Raphson iterative method was used. Alternatively, the Secant (Quasi-Newton) method, with a high number of time steps, was adopted to follow the post-peak behaviour, but the development of the rocking mechanism was not accurately described. In case of nonlinear elastic constitutive law, the shear failure of the interface and post-peak behaviour were obtained without any convergence issue adopting the Newton-Raphson iteration method, although the value of the peak lateral force was not accurately estimated. In Figure 7(b) the capacity curves for different values of the maximum shear stress are compared to each other.

Figure 8 shows the results of the 3D-model compared with those obtained by Rots and the results of the experimental test (Rots et al. 1997). The adoption of solid elements required an additional computational effort compared to the 2D- model. Especially, an associated plasticity was adopted to improve the robustness of the model by setting the dilatancy angle equal to the friction value. The model adopting the nonlinear elastic law for the interface elements gives larger global capacity of the flanged wall as compared to the corresponding 2D analyses.

In conclusion, the use of the nonlinear elastic constitutive law considered in this work allows to overcome the convergence issues of the Coulomb friction failure model, thanks to the diagonal stiffness matrix governing the interface response. On the other hand, the decoupling of the normal and tangential constitutive laws approximates the physical behaviour of the joint, so that an accurate calibration of the mechanical parameters is required (Fusco et al. 2022).

3. Analytical approach

In this section, an analytical procedure defined to evaluate the capacity curve of the pier-main wall system is presented and discussed. Section 3.1 briefly recalls the approach commonly adopted, i.e. the limit analysis method, which provides the maximum in-plane force capacity of the pier-wall system, but does not allow to follow the evolution of the nonlinear mechanisms leading to the force-displacement nonlinear response curve. Section 3.2

Table 2. Geometry and load conditions of the pier-main wall system.

Elastic modulus	E	3264	N/mm^2
Wall thickness	l_w	265	mm
Half-wall length	s_w	800	mm
Pier length	l_p	600	mm
Pier thickness	s_p	100	mm
Height	h	2500	mm
Vertical Load	q	301.9	kN/m
Unit Mass	ρ	1800	kg/m3

introduces the basic concepts of PREcast Seismic Structural System (PRESSS) rocking dissipative technology and the Monolithic Beam Analogy (MBA) procedure to model the rocking mechanism of deformable bodies. The proposed analytical method is described in section 3.3. An additional procedure to consider the compressive crushing of the pier toes is discussed in section 3.4.

The results of the analytical method are compared with those experimentally obtained by Raijmakers and Van der Pluijm (1992), and already described in the previous section. Table 2 summarizes the geometry of pier-main wall system and the applied loads, that is the vertical load at the top of the wall and the weight of the elements. Only half structure is considered to simplify the calculation due to the symmetry conditions.

3.1. Classical approach based on limit equilibrium analysis

In common practice, the limit analysis is typically used to evaluate the limit load associated with the rocking mechanism of a wall or a pier. In this approach, wall and pier are considered as rigid blocks, which rotate around the toe of the pier due to the horizontal force applied at the top of the wall, while the resultant of the compressive forces is assumed applied at the toe of the pier. The capacity of the structure is defined as the horizontal load at the top of the wall for which the rotational equilibrium is satisfied.

The self-weight of the pier and the wall (P_p and P_w) are applied at the respective centers of gravity. The resultant of the vertical loads F_v is positioned at the center of the top of the wall. As mentioned above, the compressive resultant of the base section R is applied at the toe of the pier. Several codes and guidelines assume the centre of rotation around compressed toe located in the centroid of the stress diagram. In this work, this aspect is neglected and the position of the resultant force is approximately located at the toe of the pier, as a small difference in terms of capacity is expected. It should be noted that this assumption is not conservative, so that a refinement of the analysis may be needed in case the lateral force demand is close to the capacity of the connection.

The capacity of the structure is calculated by imposing the rotational equilibrium at the limit state, i.e. before the overturning of the structure around the toe corner (pivot point), as follows:

$$F_h h = (P_w + F_v)\left(\frac{l_w}{2} + l_p\right) + P_p \frac{l_p}{2} \qquad (2)$$

In the analyzed case, the horizontal force F_h is obtained equal to 26.5 kN.

The limit analysis is typically used to calculate the overturning of the pier/wall and the capacity F_h is assumed related to a displacement equal to zero. The post-peak is characterized by the decrease of the capacity due to the *P-Delta* effect, until the overturning of the pier. Instead, in this case, since the values of the horizontal displacements are low, the *P-Delta* effect is considered negligible and the maximum capacity is assumed as constant, as illustrated in Figure 14. In conclusion, the limit analysis provides an upper bound of the horizontal capacity, which does not completely represent the evolution of the nonlinear behavior of the structure during the rocking mechanism.

3.2. Member compatibility (Monolithic Beam Analogy — MBA)

To improve the seismic performance of the structure and reduce the costs of the damage after an earthquake, a low-damage technology named PRESSS Technology was developed in the 1990s (Priestley et al. 1999). It is based on the concept of *ductile jointed connection*, where the inelastic demand is concentrated at the critical section through opening and closing of an existing gap at the interface (rocking motion of the beam or wall panel). In particular, the precast elements are connected through unbonded post-tensioned tendons. In the *hybrid system*s, the unbonded tendons and the axial load provide recentring properties, while the dissipating contribution is provided by mild steel or external replaceable dissipation devices (Pampanin 2005; Pampanin, Priestley, and Sritharan 2001).

Due to the opening and closing of the gap associated with the rocking motion, the strain compatibility of the section is violated. Thus, the relation between the strain of the concrete and neutral axis position is not valid anymore. To overcome this problem, Pampanin, Priestley, and Sritharan (2001) and Palermo (2004) proposed a relation between the imposed rotation θ_{imp} and the virtual curvature χ, enforcing a displacement compatibility at the element level, based on the Monolithic Beam Analogy (MBA). The MBA expresses in terms of global displacements the analogy between a ductile connection and an equivalent monolithic connection, as illustrated in Figure 9. In this procedure, the distribution of the plastic curvature of a monolithic reinforced concrete is assumed concentrated in the plastic hinge. Several relations are obtained depending on the displacement Δ of the point of contraflexure (Palermo 2004). The displacement and curvature at the decompression point are indicated by Δ_{dec} and χ_{dec}, and Δ_y is the displacement at the yielding point of the monolithic section. The cantilever length, L_{cant}, is the distance from the interface and the point of contraflexure, which is equal to the height of the cantilevered wall. The following relations hold:

(1) If $0 \leq \Delta \leq \Delta_{dec}$:

$$\Delta_{imp} = \Delta_{mon} = \chi_{dec} \frac{L_{cant}^2}{3} \qquad (3)$$

In this case, θ_{imp} is zero.

(2) If $\Delta_{dec} \leq \Delta \leq \Delta_y$:

$$\Delta_{imp} = \theta_{imp} L_{cant} + \chi_{dec} \frac{L_{cant}^2}{3} \qquad (4)$$

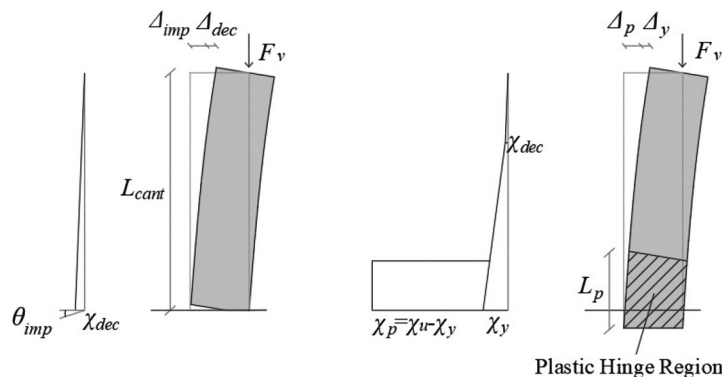$$\Delta_{mon} = \chi_{mon} \frac{L_{cant}^2}{3} \qquad (5)$$

Figure 9. Monolithic beam analogy for reinforced concrete elements (Palermo 2004).

Imposing the equivalence of the displacements, the equivalent curvature is obtained as:

$$\Delta_{imp} = \Delta_{mon} \tag{6}$$

$$\chi_{mon} = 3\frac{\theta_{imp}}{L_{cant}} + \chi_{dec} \tag{7}$$

(3) If $\Delta_y \le \Delta \le \Delta_s$:

The displacement of the monolithic concrete element is composed of an elastic and a plastic part, where L_p is the length of the plastic hinge, resulting as:

$$\Delta_{mon} = \Delta_y + \Delta_p \tag{8}$$

$$\Delta_{mon} = \chi_y \frac{L_{cant}^2}{3} + \left(\chi_y - \chi_{dec}\right)L_p\left(L_{cant} - \frac{L_p}{2}\right) \tag{9}$$

Imposing $\Delta_{imp} = \Delta_{mon}$, the equivalent curvature is:

$$\chi_{mon} = \frac{\frac{3\theta_{imp}}{L_{cant}} - \left(\chi_y - \chi_{dec}\right)}{\frac{3L_p}{L_{cant}}\left(1 - \frac{L_p}{2L_{cant}}\right)} + \chi_y \tag{10}$$

The aforementioned relations describe the curvature of a section as a function of the imposed rotation. The compression strain in the concrete measured at the outer fiber is calculated as follows:

$$\varepsilon_c = c\,\chi_{mon} \tag{11}$$

where c is the neutral axis position of the section. Imposing the rotation of the section, with an iterative procedure, it is possible to find the neutral axis position that verifies the section equilibrium. Therefore, the step-by-step moment-rotation capacity curve of the rocking interface may be evaluated. Adding the elastic (flexure and shear) deformation contribution of the element, the force–displacement curve can be obtained.

3.3. Proposed analytical procedure

The procedure here proposed is an extension of the MBA to URM U-shaped walls and is divided into three different steps. The first step regards the evaluation of the force–displacement curve of the pier-main wall system assuming that the vertical interface remains intact. The second step estimates the horizontal displacement at which the failure of the vertical interface occurs. The third step considers the pier and wall as a coupled system after the interface failure. The procedure is summarized in Figure 10.

3.3.1. Rocking mechanism

The first step of the analytical procedure aims to obtain the force–displacement curve of the pier-main wall system when the vertical connection is considered as rigid. The horizontal force applied at the top of the wall, which represents the seismic load, determinates the overturning moment of the system. The rotational equilibrium is satisfied thanks to the stabilized moment provided by the axial loads, i.e. the weight of the components and the vertical load of the floors. Unlike the limit analysis, the adopted MBA procedure considers wall and pier as a "quasi-rigid" (in fact deformable) body, with a neutral axis position instead of a pivot point at the corner toe as per the traditional rigid body rocking motion theory developed by Housner (1963).

To calculate the capacity of the pier-main wall system in terms of horizontal force and displacement, the procedure is divided into two sub-steps, as shown in Figure 11. The first sub-step evaluates the moment-rotation curve (M, θ) of the base section of the pier-main wall, rather than the traditional moment-curvature of the pier. In particular, the cracking of the section at the bottom of the system is expected due to the low value of tensile strength of the masonry and axial load ratio. Since, after the cracking, infinitive values of the
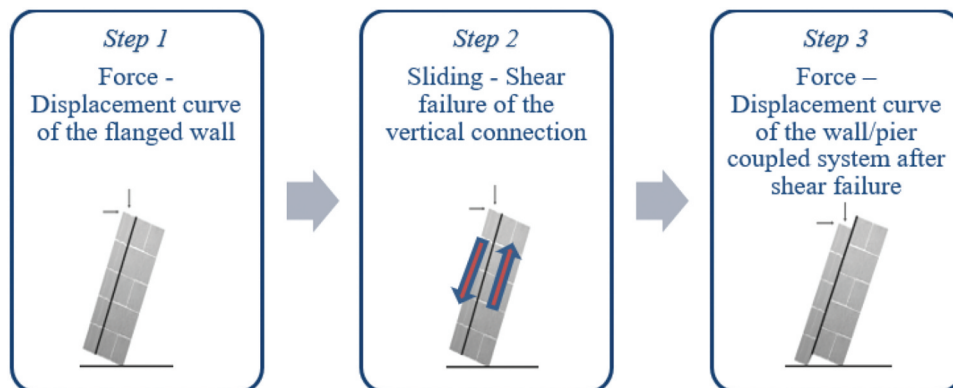

Figure 10. Conceptual steps of the analytical method to model the flanged wall as single or coupled elements.
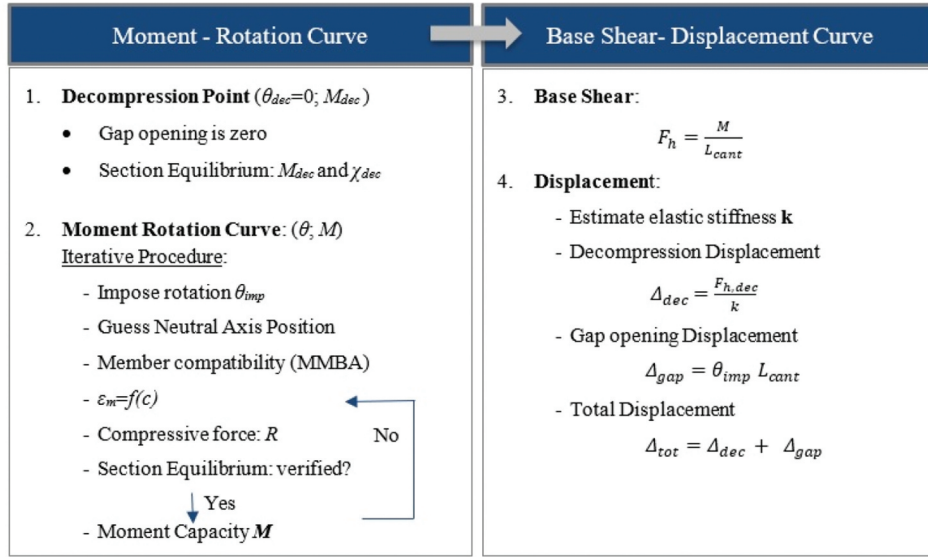
Figure 11. Flow chart force–displacement curve of the flanged wall.

curvature at the critical section would be obtained, the rotation θ is adopted as the parameter to describe the response of the critical section, as for the controlled rocking system. The relation between the (gap opening) base rotation and the compression strain in the masonry is given by the compatibility at the member level, as described in section 3.2. The position of the neutral axis and the relative moment are computed by enforcing the equilibrium of the section at any increasing value of the rotation.

The second sub-step correlates the moment-rotation curve of the base section with the force–displacement curve ($F_h - \Delta_{tot}$) of the entire system. In detail, the horizontal force is obtained by dividing the moment by the cantilever length, whereas the displacement is given by the sum of the elastic (flexure and shear contribution) displacement and the inelastic displacement determined by the rotation of the section.

Sub-step 1: Moment–Rotation Curve

In this section, the procedure to obtain the moment–rotation curve is discussed in detail. The behaviour of the section can be distinguished in the elastic phase, which precedes the base cracking (decompression point), and in the subsequent inelastic phase.

The cracking point, which is the first point of the moment–rotation curve, corresponds to zero value of the (gap opening) base rotation ($\theta_{dec} = 0$). If the tensile strength of the masonry is neglected, the position of the neutral axis is assumed to be located at the extreme fibre of the section, as illustrated in Figure 12.

The diagram of the compressive stresses at the base section is divided into three blocks to consider the different thicknesses of the wall and pier. The value of the
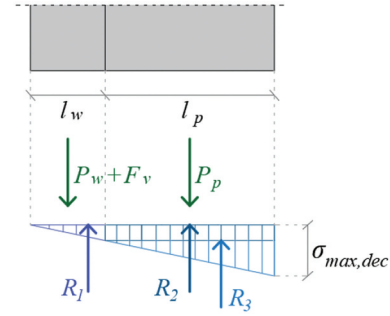
Figure 12. Internal actions of the section at the bottom: decompression point.

variable, $\sigma_{max,dec}$, is determined through the equilibrium of the vertical loads, where R_1, R_2, R_3 are the resultants of the compressive stress diagram. The moment capacity of the section related to the decompression of the base section results as:

$$M_{dec} = R_1\left(l_p + \frac{l_w}{3}\right) + R_2\frac{l_p}{2} + R_3\frac{l_p}{3} + (F_v + P_w)\left(l_p + \frac{l_w}{2}\right) + P_p\frac{l_p}{2} \quad (12)$$

Assuming a linear elastic constitutive law for the masonry, the curvature at the decompression point is expressed by Equation (13).

$$\chi_{dec} = \frac{\sigma_{max,dec}}{E(l_w + l_p)} \quad (13)$$

After the decompression point, the opening of the gap at the bottom of the wall occurs. The analytical procedure to derive the moment–rotation curve consists in finding the moment capacity of the section imposing the rotation (θ_{imp}). For each value of the imposed rotation, the position of the neutral axis is obtained according to the

following iterative procedure, based on the verification of the equilibrium of the section. Two different cases are considered corresponding to the neutral axis at the base section located in the wall and in the pier. A scheme of the strains and compressive stresses of the section are illustrated in Figure 13.

The maximum strain, defined through the member compatibility condition, is given by Equation (14). Unlike concrete, in a masonry wall no plastic hinges develop, so that the equivalent connection remains elastic. For this reason, the pre-yielding equivalent curvature is herein assumed as the most appropriate.

$$\varepsilon_{max} = -c\left(3\frac{\theta_{imp}}{L_{cant}} + \chi_{dec}\right) \qquad (14)$$

The cantilever length, L_{cant}, is the distance from the interface and the point of contraflexure, which in this specific case is equal to the height of the (cantilever) wall. Since the masonry is assumed to be linear elastic in compression, the maximum stress can be determined straightforward via the following expression:

$$\sigma_{max} = E\varepsilon_{max} \qquad (15)$$

The position of the neutral axis is obtained through the equilibrium of the vertical forces. Finally, the moment capacity is given by the contribution of the vertical loads (M_{axial}) and the moment derived from the compressive stresses (M_{comp}), resulting as:

$$M_{axial} = (F_v + P_w)\left(l_p + \frac{l_w}{2}\right) + P_p\frac{l_p}{2} \qquad (16)$$

$$M_{comp} = \begin{cases} R_1\left(l_p + \frac{(c-l_p)}{3}\right) + R_2\frac{l_p}{2} + R_3\frac{l_p}{3} & if\ c> l_p \\ R_3\frac{c}{3} & if\ c< l_p \end{cases} \qquad (17)$$

$$M = M_{axial} + M_{comp} \qquad (18)$$

Repeating this procedure iteratively for each rotation value, the moment–rotation curve of the section at the bottom of the pier-main wall is obtained interpolating the points, as illustrated in Figure 14(a).

Sub-step 2: Base Shear–Displacement Curve

The second sub-step consists in the definition of the base shear–displacement curve for the entire wall, starting from the moment–rotation curve. In detail, the lateral load capacity is obtained by dividing the moment capacity by the cantilever length, which in this case corresponds to the height of the wall.

$$F = \frac{M}{L_{cant}} \qquad (19)$$

The displacement at the top of the wall is calculated as sum of the elastic displacement Δ_{dec} and of the inelastic displacement Δ_{gap} caused by the gap opening, resulting as:
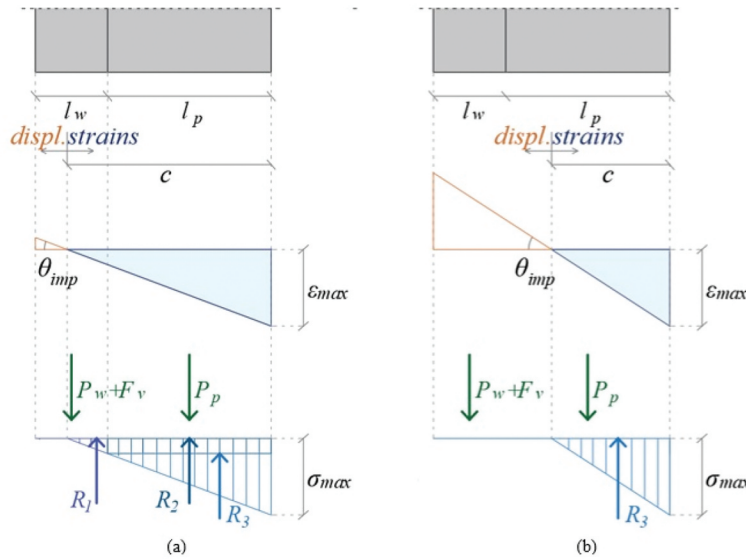

Figure 13. Strain and stress distributions at the base section: neutral axis in the wall (a) and in the pier (b).
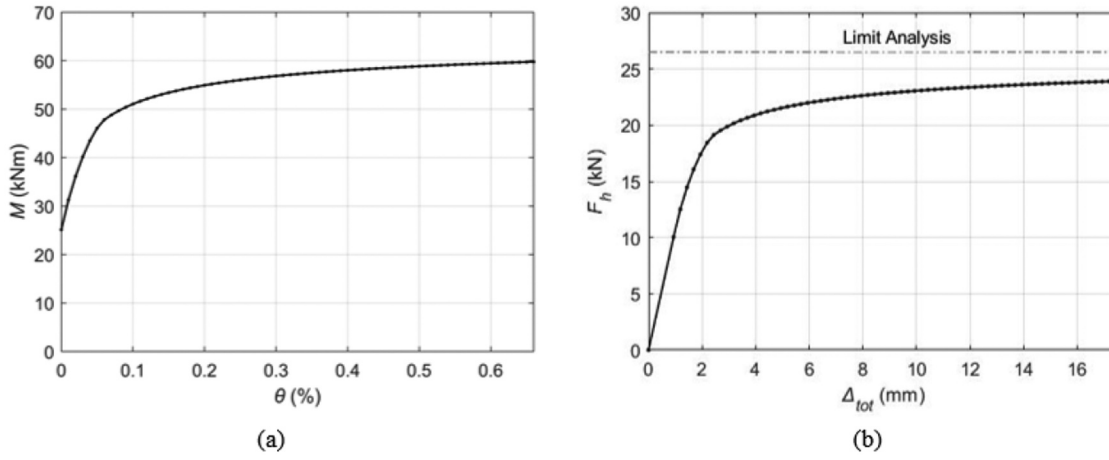
Figure 14. Moment-Rotation of the section at the bottom of the flanged wall (a) and force–displacement curve of the flanged wall (b).

$$\Delta_{dec} = \frac{F_{dec}}{k} \tag{20}$$

$$\Delta_{gap} = \theta_{imp} L_{cant} \tag{21}$$

$$\Delta_{tot} = \Delta_{dec} + \Delta_{gap} \tag{22}$$

where k is the stiffness of the half flanged wall, considering both flexural and shear contributions.

The force-displacement capacity curve of half flanged wall is shown in Figure 14(b) and compared with the results of the limit analysis. The development of the rocking mechanism is fully captured by the proposed analytical procedure, unlike the limit analysis which neglects the pre-peak flexural behavior. Also whilst the MBA considers the actual neutral axis position, the limit analysis assumes the corner toe as pivot point for the rocking mechanism, thus (un-conservatively) overestimating the level arm and overall capacity of the system.

3.3.2. Shear failure of the pier-wall connection

The shear failure of the vertical connection between the pier and wall is governed by the Mohr–Coulomb failure criterion. Consequently, the shear capacity depends on the distribution of shear and normal stresses along the vertical connection, which is highly complex to obtain analytically, due to the considerable extension of the D-region. Accordingly, a simplified global procedure based on two steps to evaluate the failure of the connection is hereinafter proposed. The first step verifies if the failure occurs, in particular if the maximum shear stress exceeds the estimated shear strength. The second step concerns the identification of the displacement at which the failure occurs and the horizontal force is then derived indirectly from the force–displacement curve. The following paragraphs describe the assumptions of the simplified proposed procedure.

The maximum shear transferred by the vertical connection (V) is assumed to be equal to the sum of the vertical load at the top of the wall and the weight of the wall. This corresponds to the phase when the wall is completely lifted, and the vertical loads are supported by the pier through the vertical connection, resulting:

$$V = F_v + P_w \tag{23}$$

In analogy with a rectangular section and in a conservative manner, the distribution of the shear stress is assumed as parabolic. Consequently, the maximum shear stress is calculated with the following expression, where A_{interf} denotes the area of the vertical joint:

$$\tau_{max,ext} = \frac{3}{2} \cdot \frac{V}{A_{interf}} \tag{24}$$

As previously mentioned, due to the difficulty of calculating the normal stress distribution along the connection, a further conservative assumption is adopted. Namely, the frictional contribution to the resisting shear stress is assumed to be negligible, so that the strength only depends on the cohesion $\tau_{cohesion}$, that is:

$$\tau_{res} = \tau_{cohesion} \tag{25}$$

Once the maximum shear stress along the joint exceeds the shear strength (Equation 25), the failure of the vertical connection occurs being:

$$\tau_{max,ext} \geq \tau_{res} \tag{26}$$

When Equation (25) is verified, a straight line is drawn in the force-displacement diagram, as illustrated in Figure 15, which represents the failure of the vertical connection. The horizontal displacement at the top of the wall of this line corresponds to the value for which the wall is completely lifted. In fact, from the procedure
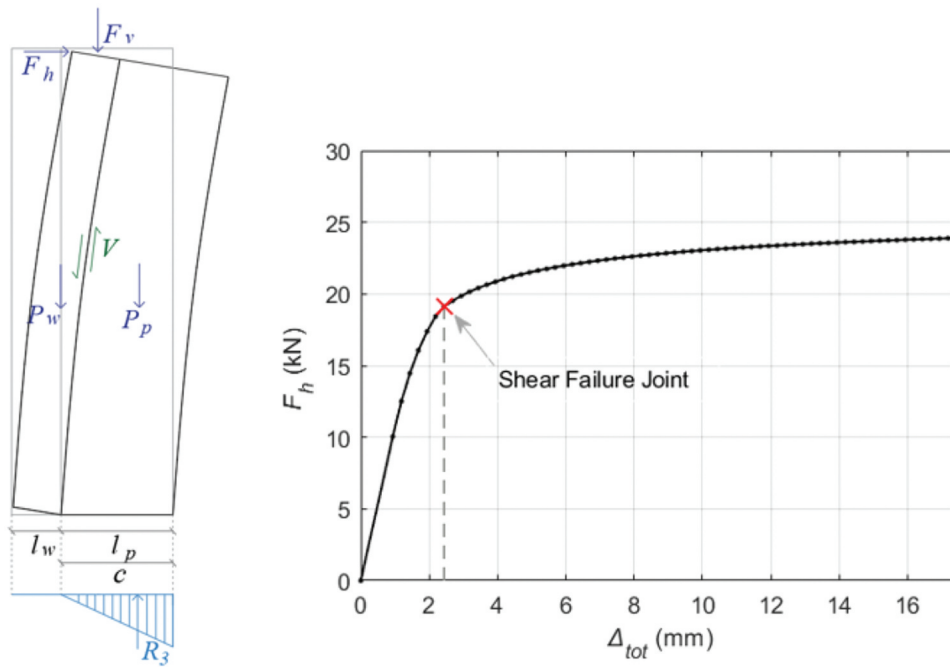
Figure 15. Failure of the vertical connection.

of the flanged wall capacity curve, it is possible to know the position of the neutral axis at each value of the horizontal displacement. Therefore, the value of this for which the neutral axis passes from the wall to the pier is considered as the horizontal displacement related to the sliding. If Equation (26) is not verified, the original force–displacement curve computed from section 3.3.1 can be used (up to the toe crushing).

3.3.3. Rocking mechanism after the sliding shear failure at the interace

In case of sliding shear failure of the vertical interface, the response can be analytically described and modelled assuming a complete degradation of the cohesive bond between wall and pier, which remain only coupled via the residual friction of the interface, as shown in Figure 16(a). The behaviour of the coupled system is
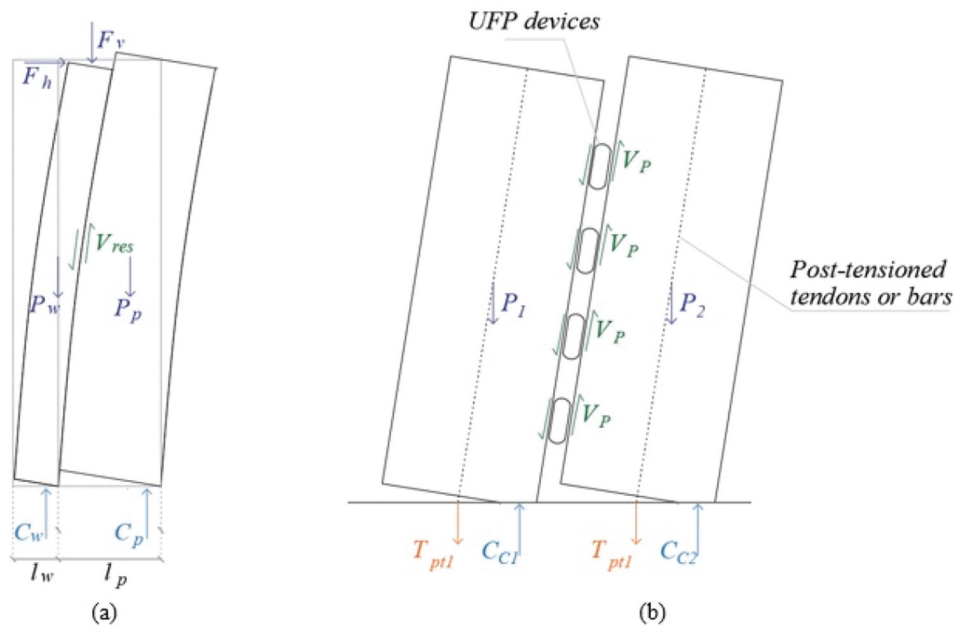
Figure 16. Equilibrium of the coupled pier-wall (a) and an example of a coupled post-tensioned rocking wall via U-shaped flexural plates (NZCS 2010).

hereinafter described in analogy with the analytical procedure used for coupled post-tensioned rocking walls via U-Shaped Flexural Plates illustrated in Figure 16(b).

The overturning moment is obtained as sum of the moment capacity of wall, M_w, and the pier, M_p, calculated about the centre of the sections of each structural component, and an additional contribution related to the coupling shear V_{res}, resulting as:

$$M_{ot} = M_w + M_p + V_{res}\left(\frac{l_w + l_p}{2}\right) \qquad (27)$$

The moment capacities M_w and M_p are obtained by imposing the rotational equilibrium at the base section, considering the contribution of the residual shear transferred via the connection, in case the resultant force interface demand exceeds the Coulomb force capacity, as illustrated in Figure 16. The equilibrium expressions for the wall and pier are reported in Equation (28) and Equation (29), respectively, where C_w and C_p are the resultant compression forces, as follows:

$$C_w + V_{res} - P_w - F_v = 0 \qquad (28)$$

$$C_p - V_{res} - P_p = 0 \qquad (29)$$

The analytical procedure is summarized in Figure 17. The coupling shear force transferred through the interface is assumed to be equal to the residual friction of the connection. Namely, the value of the coupling force is a function of the stresses normal to the interface and the friction coefficient. As mentioned in the previous section, the distribution of the normal stresses along the connection is complex and onerous to be estimated analytically. For this reason, a simplified expression to evaluate the shear force is proposed. The shear force is assumed to be equal to the friction coefficient of the joint, μ, multiplied by the lateral load capacity, obtained through the limit analysis $F_{h,lim}$. In this case, the interface shear results are equal to 19.9 kN, considering the friction coefficient μ and the lateral force $F_{h,lim}$ equal to 0.75 and 26.5 kN, respectively. It results:

$$V_{res} = \mu F_{h,lim} \qquad (30)$$

The resultant of the coupling shear force is proportional to the maximum lateral force computed via the limit analysis, which is an upper bound for the lateral capacity of the wall. For this reason, also the coupling shear, and therefore the overall capacity of the wall obtained through Equation (30), is considered an upper bound of the real capacity. On the opposite, the lower bound is obtained by assuming $V_{res} = 0$. The analytical procedure defined to obtain the moment

capacity of the wall is hereinafter explained for the upper bound curve only.

This computes first the moment–rotation curve of the section at the base of the U-wall. As shown in section 3.3.1, for each value of the imposed rotation $\theta_{imp,w}$, the neutral axis c_w position is iteratively computed. Assuming a linear elastic constitutive law, the position of the neutral axis c_w is calculated via the equilibrium of the wall section expressed in Equation (28). Consequently, the moment capacity of the wall is:

$$M_w = C_w\left(\frac{l_w}{2} - \frac{c_w}{3}\right) \qquad (31)$$

The same procedure is repeated to compute the moment-rotation of the pier. For each imposed rotation $\theta_{imp,p}$, the position of the neutral axis c_p is obtained by imposing the equilibrium of the section in Equation (29) and the moment capacity of the pier is given by:

$$M_p = C_p\left(\frac{l_p}{2} - \frac{c_p}{3}\right) \qquad (32)$$

The displacement at the decompression point is calculated as follows:

$$\Delta_{dec,w} = \chi_{dec,w}\frac{L_{cant}^2}{3} \qquad (33)$$

The displacement related to the gap opening is computed via the following expression:

$$\Delta_{gap,w} = \theta_{imp,w}L_{cant} \qquad (34)$$

Finally, the total displacement is:

$$\Delta_{tot,w} = \Delta_{dec,w} + \Delta_{gap,w} \qquad (35)$$

The lateral load capacity of the wall is obtained by dividing the moment capacity by the cantilever length as follows:

$$F_{h,w} = \frac{M_w}{L_{cant}} \qquad (36)$$

The same procedure is applied to compute the force–displacement curve of the pier.

The additional contribution of the coupling shear is estimated as described above and by assuming a constant shear force. This results as:

$$M_V = V_{res}\left(\frac{l_w + l_p}{2}\right) \qquad (37)$$

$$F_{h,V} = \frac{M_V}{L_{cant}} \qquad (38)$$

Finally, the force–displacement curve of the coupled wall-pier is obtained by summing up the moment capacity of pier and wall and the contribution of the coupling shear:
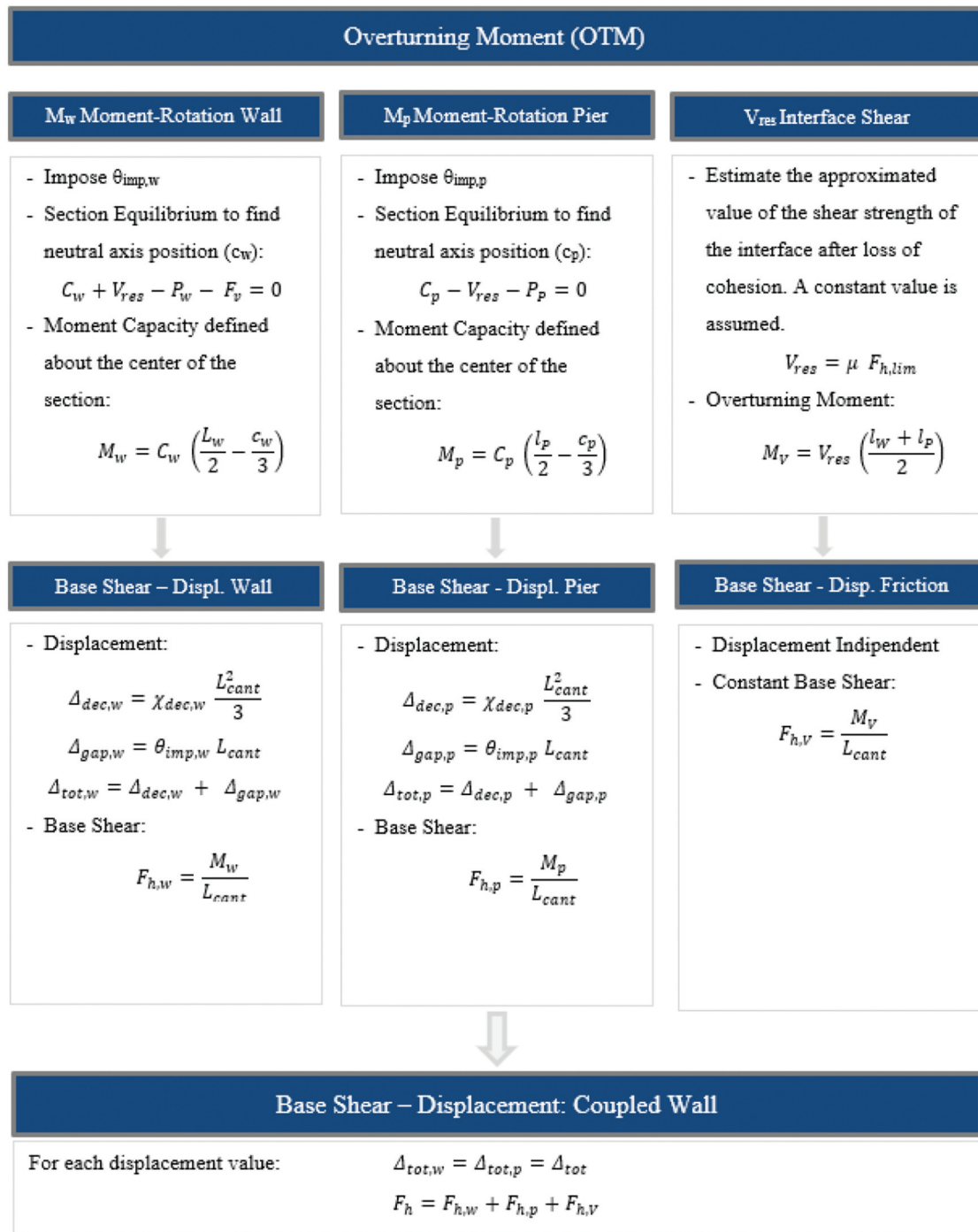
Overturning Moment (OTM)

M_w Moment-Rotation Wall

- Impose $\theta_{imp,w}$
- Section Equilibrium to find neutral axis position (c_w):

$$C_w + V_{res} - P_w - F_v = 0$$

- Moment Capacity defined about the center of the section:

$$M_w = C_w \left(\frac{L_w}{2} - \frac{c_w}{3}\right)$$

M_p Moment-Rotation Pier

- Impose $\theta_{imp,p}$
- Section Equilibrium to find neutral axis position (c_p):

$$C_p - V_{res} - P_p = 0$$

- Moment Capacity defined about the center of the section:

$$M_p = C_p \left(\frac{l_p}{2} - \frac{c_p}{3}\right)$$

V_{res} Interface Shear

- Estimate the approximated value of the shear strength of the interface after loss of cohesion. A constant value is assumed.

$$V_{res} = \mu \ F_{h,lim}$$

- Overturning Moment:

$$M_V = V_{res} \left(\frac{l_w + l_p}{2}\right)$$

Base Shear – Displ. Wall

- Displacement:

$$\Delta_{dec,w} = \chi_{dec,w} \frac{L_{cant}^2}{3}$$

$$\Delta_{gap,w} = \theta_{imp,w} L_{cant}$$

$$\Delta_{tot,w} = \Delta_{dec,w} + \Delta_{gap,w}$$

- Base Shear:

$$F_{h,w} = \frac{M_w}{L_{cant}}$$

Base Shear - Displ. Pier

- Displacement:

$$\Delta_{dec,p} = \chi_{dec,p} \frac{L_{cant}^2}{3}$$

$$\Delta_{gap,p} = \theta_{imp,p} L_{cant}$$

$$\Delta_{tot,p} = \Delta_{dec,p} + \Delta_{gap,p}$$

- Base Shear:

$$F_{h,p} = \frac{M_p}{L_{cant}}$$

Base Shear - Disp. Friction

- Displacement Indipendent
- Constant Base Shear:

$$F_{h,V} = \frac{M_V}{L_{cant}}$$

Base Shear – Displacement: Coupled Wall

For each displacement value:

$$\Delta_{tot,w} = \Delta_{tot,p} = \Delta_{tot}$$

$$F_h = F_{h,w} + F_{h,p} + F_{h,V}$$

Figure 17. Flow chart force–displacement curve of the coupled pier-wall after shear failure of the vertical connection.

$$F_h = F_{h,w} + F_{h,p} + F_{h,V} \tag{39}$$

The results are illustrated in Figure 18. The upper bound of the capacity curve corresponds to the coupling shear proportional to the maximum lateral force computed via the limit analysis. On the opposite, the lower bound is calculated by imposing a zero residual shear force along the interface.

The upper-bound capacity curve of the coupled wall is different from zero for a horizontal displacement equal to zero. It is evident that it has no real physical meaning, but it is caused by the assumption of considering the shear force as constant. Since the coupling of wall and pier only occurs after the failure of the connection, the initial branch of this curve is not relevant if considered alone, but should rather be part of a two-stage
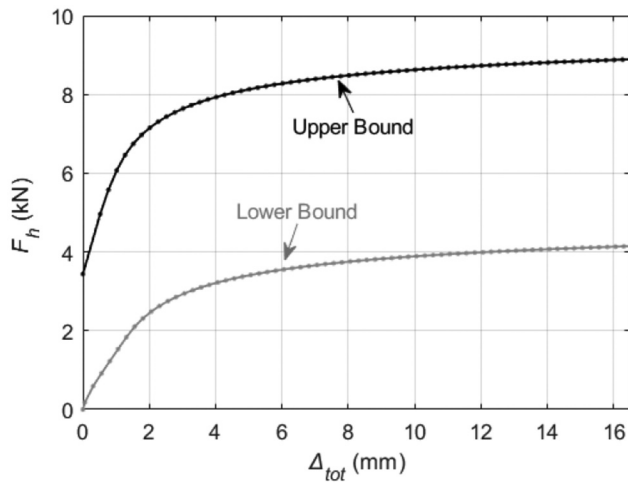
Figure 18. Capacity curve of the coupled wall/pier: upper and lower bound.

analysis merging the initial phase (fully coupled pre-sliding) and the final stage (sliding shear at the interface and residual coupling friction shear) as described in the following section, where a consolid analytical approach is proposed and validated against the numerical results.

3.4. Comparison between the analytical and experimental results

In the previous sections, half structure was considered due to symmetry. The capacity curve of the whole U-wall system is obtained by multiplying by two the horizontal force, as shown in Figure 19. This illustrates the capacity curve of a flanged wall with an intact interface connection, the upper and lower bound of the capacity curve of the coupled pier-wall after shear
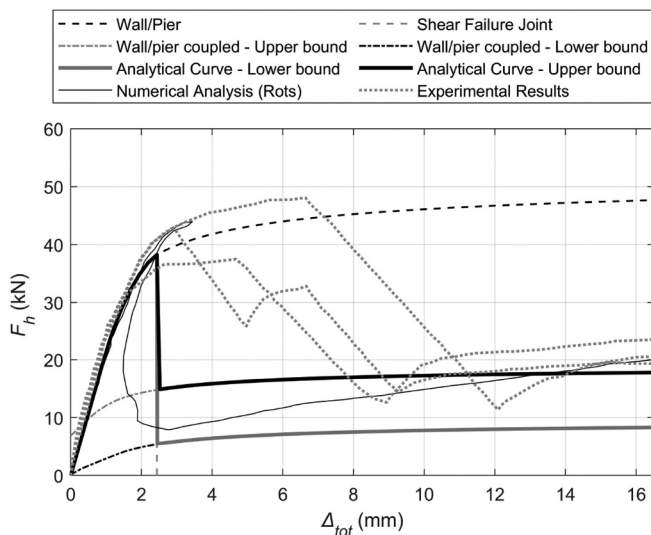

Figure 19. Numerical analysis vs analytical analysis results.

failure, and the horizontal displacement for which the failure of the connection occurs. The behaviour of the U-wall is represented by the combination of the two phases of the mechanism (pre- and post- interface sliding): the black thick curve represents the upper-bound curve and the grey thick curve indicates the lower bound curve. For both curves, the initial capacity coincides with that of the pier-wall with a rigid connection (dashed black curve) up to the displacement at which the failure of the interface connection occurs (dashed grey curve). The sliding failure of the joint reduces the capacity of the U-wall down to intersect the dash-dotted curves, which represent the upper and lower bound behaviour of the wall/pier after the sliding Figure 19 compares the capacity curve obtained via the experimental/numerical simulations and the analytical capacity curve. The numerical results are presented in (Rots et al. 1997) and validated by comparison with the results of the experimental test. The analytical model is able to predict accurately the stiffness degradation due to the onset of the rocking mechanism. However, the failure of the vertical connection occurs for both lower horizontal displacements and lateral forces in the case of the analytical model with respect to the numerical results. As regards the post-peak behaviour, the numerical model shows an increase of the lateral force due to the increase of the normal stresses along the interface, caused by the increasing imposed displacements. This specific behaviour is not described by the analytical model, which assumes a constant shear force transferred along the connection, so that the lateral force after the peak remains approximately constant. On the other hand, the numerical curve remains mostly within the lower and upper bounds estimated via the analytical method. The analytical procedure is therefore able to provide a simple but sufficiently accurate prediction of the U-wall force–displacement curve.

3.5. Accounting for toe-crushing failure in the analytical procedure

The compressive failure, characterized by sub-vertical cracks, was observed in a several real earthquakes (Parisi and Augenti 2013a). Several alternative procedure to consider the compression failure in the section analysis is also present in the literature (Parisi and Augenti 2013b). In this section, the previously proposed analytical method is refined by including also the toe-crushing of the pier as a potential failure mechanism, caused by the compressive stress localization at the bottom due to rocking. Such a failure mechanism can occur when large compressive forces are transferred at the base

of the wall, and it occurs then when the vertical connection does not fail. For this reason, a rigid vertical connection is assumed in the following.

With respect to the procedure described in the previous sections, a parabolic nonlinear constitutive law for masonry is used (Figure 20(a)). For the considered wall, the maximum compressive stress is equal to 5.9 N/mm² and the ultimate strain to 0.5%, based on common literature (Jafari, Esposito, and Rots 2019).

Similar to the procedure described in section 3.3.1 for the rocking mechanism, the position of the neutral axis is obtained from the section equilibrium, and the moment capacity is then calculated. To consider a nonlinear constitutive law, the problem is discretized and the section is divided into equal intervals Δx, as illustrated in Figure 20(b). The values of the strain at each point of the discretization are calculated by:

$$\varepsilon_i = \varepsilon_{max}\left(\frac{c - (L - x_i)}{c}\right) \qquad (40)$$

Consequently, the constitutive law relates the strain to the stress as:

$$\sigma_i = f(\varepsilon_i) \qquad (41)$$

For each interval, the compressive force resultant and the moment about the extremity of the section are obtained as follows:

$$R_i = \sigma_i s \Delta_x \qquad (42)$$

$$M_i = R_i(L - x_i) \qquad (43)$$

The total resultant of the compressive force at the base and the moment derived from this are the sum of the contribution of each interval:

$$R_{com} = \sum R_i \qquad (44)$$

$$M_{com} = \sum M_i \qquad (45)$$

Therefore, R_{com} is included in the equilibrium equation, instead of $R_1 + R_2 + R_3$. Similarly, also the moment M_{com} in Equation (17) is now evaluated via Equation (45).

The remaining part of the procedure employed to obtain the force–displacement curve from the moment-rotation is identical to that described in section 3.3.1. The force–displacement curve obtained from the nonlinear constitutive law for masonry is illustrated in Figure 21 for the considered U-shaped wall (assuming that no failure of the vertical joint occurs), where the drop of the capacity at the end of the curve corresponds to the toe-crushing of the pier. In addition, diagrams of the stresses along the base section of the wall are plotted for three different imposed rotations(Figure 22). When the imposed rotation is equal to 0.05%, the neutral axis
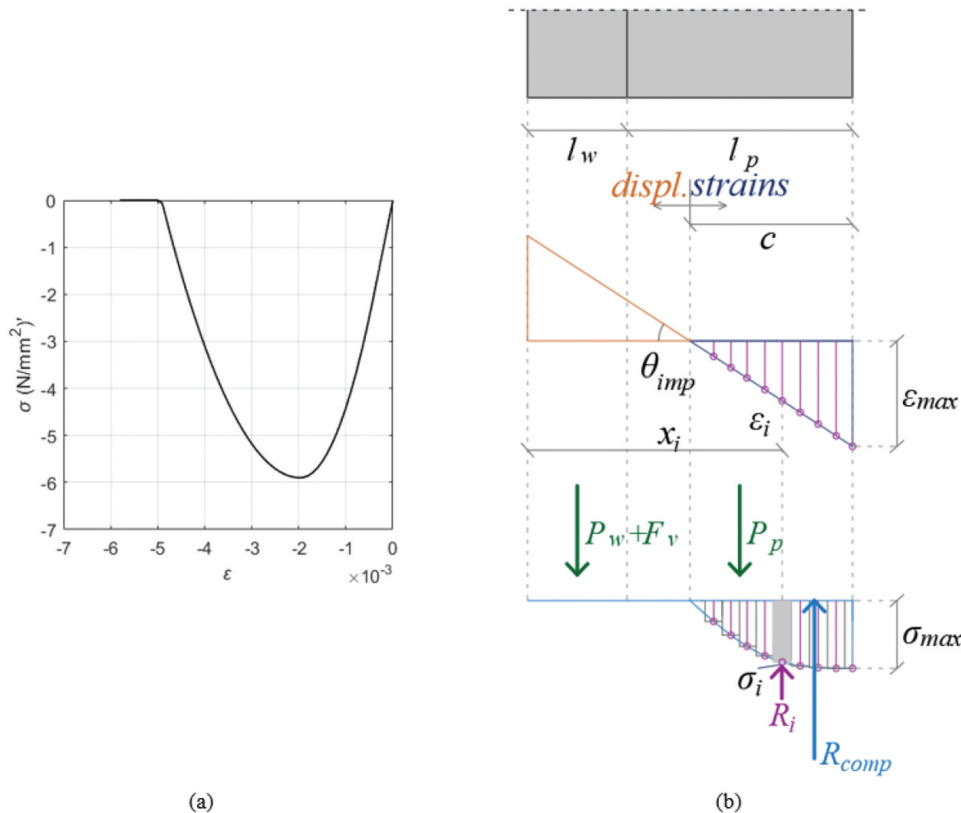

(a)
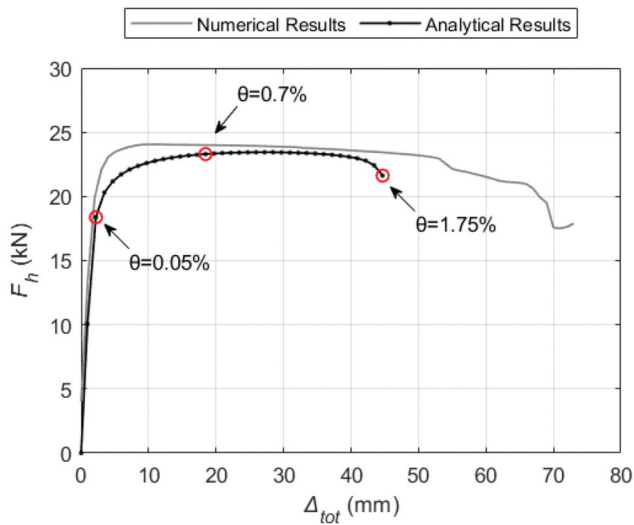
(b)

Figure 20. Masonry constitutive law and section analysis.

Figure 21. Comparison capacity curve: analytical vs numerical methods.

4. Conclusions

The seismic performance of Dutch masonry terraced houses built after the 1980s may be limited by the failure of the continuous vertical connections that are present at the corners between crossing walls and piers. In common practice, these connections are assumed to be rigid, but this assumption may lead to overestimate the lateral load capacity of the masonry buildings, especially when cohesion and friction of the connection are not sufficiently high. The present work investigates the problem via both a numerical and an analytical approach, whose limitations and advantages are discussed.

The most critical aspect of the numerical modelling of these structures is the choice of the constitutive law for the vertical continuous connections between wall and pier, which are typically modelled by means of interface elements. A Coulomb-friction criterion provides the most appropriate description of the physical behavior of the connection. However, the analyses presented in this work highlight the severe numerical convergence issues related to the brittle shear failure of the vertical connection. Therefore, a nonlinear elastic constitutive law may be considered as an alternative. This law decouples the force-displacement behaviour in the normal and tangential directions. Such assumption, although less consistent with the actual mechanical response, allows for the stability of the numerical analysis, but it requires the calibration of the mechanical parameters.

still lies in the main wall and masonry still exhibits an elastic behaviour. At $\theta_{imp} = .7\%$ the nonlinear behaviour of the material already occurs. For even larger rotations, the stresses decrease until the stress located at the toe of the pier reaches a zero value (complete toe-crushing). For the considered wall, the toe-crushing is reached for a rotation equal to 1.75%.

The analytical force–displacement curve is compared in Figure 21 to the corresponding curve defined via numerical simulations in which the vertical connection was modelled as rigid to prevent the joint shear failure. The model corresponds to that presented in Section 2, but a parabolic nonlinear constitutive law with compressive strength equal to 5.9 N/mm^2 and compressive fracture energy equal to 25 N/mm^2 was used to model the masonry. The results of the numerical simulation show a larger ductility of the wall when compared to the analytical predictions, which can therefore be used to obtain a conservative but reasonable first estimate of the displacement capacity of the wall.
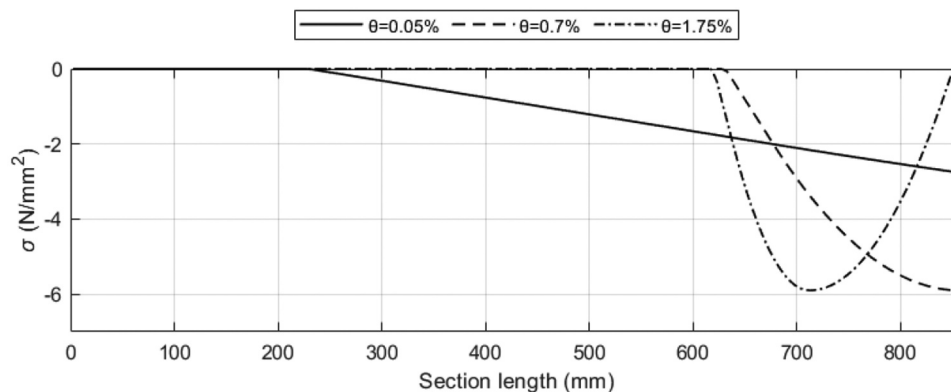
The proposed analytical procedure overcomes the limitations of limit equilibrium analysis, which can be used to estimate the capacity of the structure. The described procedure identifies three phases: first the onset of rocking of the pier-main wall system when the connection is intact, second the shear failure of the vertical connection, and third the rocking of the coupled wall-pier system in the post-peak phase. Additionally, also the toe-crushing at the bottom of the pier is

Figure 22. Stress values along the base section for three representative imposed rotations of the wall.

considered as failure mechanism alternative to the shear failure of the connection. Although the analytical nature of the model requires the definition of simplifying assumptions, the results of the analytical method are consistent with those obtained via the numerical simulations. Therefore, the proposed analytical method can be used to provide a quick, but sufficiently accurate, estimate of the complete force–displacement curve of a URM U-wall.

Acknowledgments

Disclosure statement

Daniela Fusco is employed at the company Italferr S.p.A. The results of this scientific paper are part of her MSc thesis research, carried out before the employment.

ORCID

D. Addessi http://orcid.org/0000-0003-0580-3200
F. Messali http://orcid.org/0000-0002-5525-8522

References

Addessi, D., S. Marfia, E. Sacco, and J. Toti. 2014. Modeling approaches for masonry structures. *Open Civil Engineering Journal* 8 (1):288–300. doi:10.2174/1874149501408010288.

Benedetti, A., and E. Steli. 2008. Analytical models for shear–displacement curves of unreinforced and FRP reinforced masonry panel. *Construction and Building Materials* 22 (3):175–85. doi:10.1016/j.conbuildmat.2006.09.005.

Calderini, C., S. Cattari, and S. Lagomarsino. 2008. In-plane strength of unreinforced masonry piers. *Earthquake Engineering and Structural Dynamics* 38 (2):243–67. doi:10.1002/eqe.860.

Calderini, C., and S. Lagomarsino. 2008. Continuum model for in-plane anisotropic inelastic behavior of masonry. *Journal of Structural Engineering (ASCE)* 134 (2):209–20. doi:10.1061/(ASCE)0733-9445(2008)134:2(209).

Christopoulos, C., A. Filiatrault, C. M. Uang, and B. Folz. 2002. Post-tensioned energy dissipating connections for moment resisting steel frames. *Journal of Structural Engineering (ASCE)* 128 (9):1111–20. doi:10.1061/(ASCE)0733-9445(2002)128:9(1111).

DIANA FEA User's Manual. 2019. TNO building and construction research.

Esposito, R., F. Messali, P. Ravenshorst, R. Schipper, and J. Rots. 2019. Seismic assessment of a lab-tested two-storey unreinforced masonry Dutch terraced house. *Bulletin of Earthquake Engineering* 17 (8):4601–23. doi:10.1007/s10518-019-00572-w.

Esposito, R., K. Terwel, G. Ravenshorst, R. Schipper, F. Messali, and J. Rots. 2017. Cyclic pushover test on an unreinforced masonry structure resembling a typical Dutch terraced house. 16th World Conference on Earthquake Engineering, Santiago, Chile.

Fusco, D., F. Messali, J. Rots, D. Addessi, and S. Pampanin. 2021. Numerical study of pier-wall connections in typical Dutch URM buildings. In *12th International Conference on Structural Analysis of Historical Constructions: SAHC 2021, Online event, 29 Sep - 1 Oct,2021*, ed. P. Roca, L. Pelà, and C. Molins, International Centre for Numerical Methods in Engineering, CIMNE. 2217–28.

Fusco, D., F. Messali, J. Rots, D. Addessi, and S. Pampanin. 2022. Numerical issues on brittle shear failure of pier-wall continuous vertical joints in URM Dutch buildings. *Engineering Structures* 258:114078. doi:10.1016/j.engstruct.2022.114078.

Housner, W. G. 1963. The behavior of inverted pendulum structures during earthquakes. *Bulletin of the Seismological Society of America* 53 (2):403–17. doi:10.1785/BSSA0530020403.

Jafari, S., R. Esposito, and J. G. Rots. 2019. From brick to element: Investigating the mechanical properties of calcium silicate masonry *Structural analysis of historical constructions*, edied byAguilar, R., Torrealva, D., Moreira, S., Pando, M. A., and Ramos, L. F. Vol. 18, 596–604. Cham: Springer.

Kallioras, S., L. Grottoli, and F. Graziotti. 2020. Quasi-static cyclic tests on U-shaped unreinforced masonry walls made of calcium-silicate bricks and blocks. EUCENTRE Research Report EUC092/2020U, EUCENTRE, Pavia, Italy.

Lourenco, P. B. 1996. Computational strategies for masonry structures. PhD Thesis., Delft University of Technology.

Lourenco, P. B. 2002. Computations on historic masonry structures. *Progress in Structural Engineering and Materials* 4 (3):301–19. doi:10.1002/pse.120.

Magenes, G., and A. Penna. 2011. Seismic design and assessment of masonry buildings in Europe: recent research and code development issues. 9th Australasian Masonry Conference, Queenstown, New Zealand.

Mariani, V., F. Messali, M. Hendriks, and J. Rots. 2017. Numerical modelling and seismic analysis of Dutch masonry structural components and buildings. 16th World Conference on Earthquake Engineering, Santiago, Chile.

Messali, F., M. Pari, R. Esposito, J. G. Rots, and D. Den Hertog. 2018. Blind predictions of a cyclic pushover test on a two-storey masonry assemblage: A comparative study. 16th European Conference on Earthquake Engineering, Thessaloniki, Greece.

Newcombe, M., S. Pampanin, A. Buchanan, and A. Palermo. 2008. Section analysis and cyclic behavior of post-tensioned jointed ductile connections for multi-storey timber buildings. *Journal of Earthquake Engineering* Special Issue 83-110 12 (sup1):83–110. doi:10.1080/13632460801925632.

NZCS. 2010. *PRESSS design handbook*. ed. S. Pampanin, Wellington: New Zealand Concrete Society.

Palermo, A. 2004. Use of controlled rocking in the seismic design of bridges. PhD Thesis., Technical Institute of Milan.

Palermo, A., S. Pampanin, A. Buchanan, and M. Newcombe. 2005. Seismic design of multi-storey buildings using Laminated Veneer Lumber (LVL). NZSEE National Conference, Wairakei.

Palermo, A., S. Pampanin, and A. Carr. 2005. Efficiency of simplified alternative modelling approaches to predict the seismic response of precast concrete hybrid systems. Fib Symposium *Keep Concrete Attractive*, Budapest.

Palermo, A., S. Pampanin, and D. Marriott. 2007. Design, modeling and experimental investigation of seismic-resistant bridge piers with post-tensioned dissipating connections. *Journal of Structural Engineering (ASCE)* 133 (11):1648–61. doi:10.1061/(ASCE)0733-9445(2007)133:11(1648).

Pampanin, S. 2005. Emerging solutions for high seismic performance of precast/prestressed concrete buildings. *Journal of Advanced Concrete Technology* 3 (2):207–23. doi:10.3151/jact.3.207.

Pampanin, S., M. J. N. Priestley, and S. Sritharan. 2001. Analytical modelling of the seismic behaviour of precast concrete frames Designed with ductile connections. *Journal of Earthquake Engineering* 5 (3):329–67. doi:10.1080/13632460109350397.

Parisi, F., and N. Augenti. 2013a. Earthquake damages to cultural heritage constructions and simplified assessment of artworks. *Engineering Failure Analysis* 34:735–60. doi:10.1016/j.engfailanal.2013.01.005.

Parisi, F., and N. Augenti. 2013b. Assessment of unreinforced masonry cross sections under eccentric compression accounting for strain softening. *Construction and Building Materials* 41:654–64. doi:10.1016/j.conbuildmat.2012.12.039.

Parisi, F., C. Balestrieri, and D. Asprone. 2016. Nonlinear micromechanical model for tuff stone masonry: Experimental validation and performance limit states. *Construction and Building Materials* 105:165–75. doi:10.1016/j.conbuildmat.2015.12.078.

Petry, S., and K. Beyer. 2015. Force–displacement response of in-plane-loaded URM walls with a dominating flexural mode. *Earthquake Engineering and Structural Dynamics* 44 (14):2551–73. doi:10.1002/eqe.2597.

Priestley, M. J. N., S. Sritharan, J. Conley, and S. Pampanin. 1999. Preliminary results and conclusions from the PRESSS precast 5-story test building. *PCI Journal* 44 (6):42–67. doi:10.15554/pcij.11011999.42.67.

Raijmakers, T. M. J., and R. Van der Pluijm. 1992. Stability of the calcium silicate piers. TNOBouw Report BI-91-0219.

Rots, J., R. Van der Pluijm, A. Th. Vermeltfoort, and H. J. M. Janssen. 1997. *Structural masonry: An experimental-numerical basis for practical design rules*. Rotterdam: A.A. Balkema.

Sacco, E., D. Addessi, and K. Sab. 2018. New trends in mechanics of masonry. *Meccanica* 53 (7):1565–69. doi:10.1007/s11012-018-0839-x.

Sansoni, C. 2021. Seismic vulnerability assessment of exiting URM structures through a simplified analytical method. PhD Diss., Sapienza Universityof Rome.